

Single Crystalline Magnetite Nanotubes

Zuqin Liu,[†] Daihua Zhang,[†] Song Han,[†] Chao Li,[†] Bo Lei,[†] Weigang Lu,[‡] Jiye Fang,[‡] and Chongwu Zhou^{*†}

Department of Electrical Engineering-Electrophysics, University of Southern California, Los Angeles, California 90089, and Chemistry Department and Advanced Materials Research Institute, University of New Orleans, New Orleans, Louisiana, 70148

Received September 10, 2004; E-mail: chongwuz@usc.edu

Inorganic tubular nanostructures have stimulated extensive research efforts because of their prospective applications in diverse areas including ion transport, bioseparation, drug delivery, ink-jet printing and electrochemical energy production.¹ Magnetic nanotubes (e.g., FePb,^{1c} Fe₃O₄,^{1c} and LPMO²), in particular, may potentially serve as tunable fluidic channels for tiny magnetic particles, data storage devices in nanocircuits, and scanning tips for magnetic force microscopes.³ Despite their technological importance, very limited synthetic efforts have been focused on magnetic nanotubes thus far. Moreover, the obtained products are either amorphous or semicrystalline with the conventional synthesis techniques such as template reactions, sol-gel chemistry, and hydrothermal methods.⁴ In this contribution, we report the first successful synthesis of single crystalline Fe₃O₄ nanotubes by wet-etching the MgO inner cores of MgO/Fe₃O₄ core-shell nanowires. This simple technique readily generates homogeneous Fe₃O₄ nanotubes with controllable length, diameter, and wall thickness. In addition to the wide potential applications mentioned above, these single crystalline Fe₃O₄ nanotubes are also of scientific significance as they provide templates for fundamental studies on low-dimensional magnetic systems, where novel effects such as quantum confinement and quasi-coherent nucleation are expected as the dimension is substantially shrunk and interatomic exchange is no longer negligible compared to magnetostatic interactions.⁵

Our strategy for the preparation of Fe₃O₄ nanotubes followed the three-step process depicted in Figure 1. Single crystalline MgO nanowires were first grown on Si/SiO₂ substrates. A conformal layer of Fe₃O₄ was then deposited onto the nanowires using the pulsed laser deposition (PLD) technique to obtain MgO/Fe₃O₄ core-shell nanowires. Detailed synthesis conditions of MgO nanowires and the core-shell nanowires have been described in our previous report and Supporting Information.^{6,7} Finally, the MgO inner cores of the MgO/Fe₃O₄ core-shell nanowires were selectively etched in (NH₄)₂SO₄ (Alfa Aesar, 99.99%) solution (10 wt %, pH ≈ 6.0) at a temperature of 80 °C. Etching time of ~1.5 h was typically used to obtain micrometer-long Fe₃O₄ nanotubes with completely etched inner cores. The samples were then rinsed carefully with deionized water to remove the residual contaminants in/on the Fe₃O₄ nanotubes. This etching process was verified by the scanning electron microscopy (SEM) images presented in Figure 2. Bare MgO nanowires (Figure 2a) were found to be completely removed by the etching agent (Figure 2c), while the MgO/Fe₃O₄ core-shell nanowires (Figure 2b) undergoing the identical etching process maintained their morphology, as Fe₃O₄ nanotubes were left after the MgO cores were etched away, shown in Figure 2d.

To examine the crystal structure and chemical composition of the as-prepared Fe₃O₄ nanotubes, transmission electron microscopy

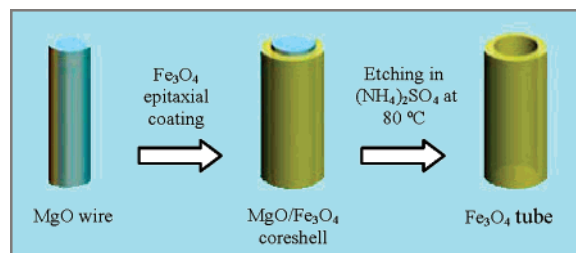


Figure 1. Schematic illustration of the fabrication process of Fe₃O₄ nanotubes.

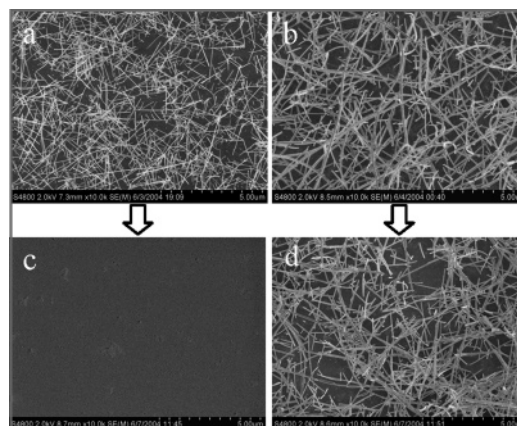


Figure 2. SEM images of MgO nanowires before (a) and after etching (c); MgO/Fe₃O₄ core-shell nanowires before (b) and after the same etching process (d).

(TEM) and energy-dispersive X-ray spectroscopy (EDS) measurements have also been conducted. A typical TEM image of an Fe₃O₄ nanotube is depicted in Figure 3a, where the contrast between the tube wall and the inside hollow region can be clearly identified. The Fe₃O₄ nanotube, around 30 nm in outer diameter, has a smooth and uniform sidewall along the whole length with a thickness of ~7 nm. One open end can be clearly seen in the image, from which the etchant entered the tube and etched up the inner material. A selected area electron diffraction (SAED) pattern was presented and indexed in the inset of Figure 3a, indicating the single-crystal nature of the nanotube. Further analysis on the SEAD pattern revealed that the nanotube has a cubic reverse spinel structure with a latticed constant of $a = 0.840$ nm, which matches the value for bulk Fe₃O₄.⁸ More information about the crystal can be derived from the high-resolution TEM (HRTEM) image taken on the side wall of the nanotube (lower inset in Figure 3a). The lattice spacing was calculated to be 0.295 nm, in good agreement with the (220) spacing of Fe₃O₄. The angle between the lattice fringe of (220) plane and the axial direction is 45°. This tells us that the growth direction is along [100]. Reducing the etching time (~20 min)

[†] University of Southern California.

[‡] University of New Orleans.

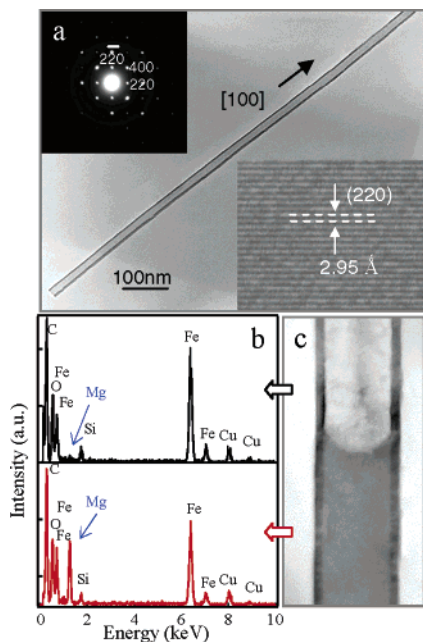


Figure 3. (a) Low-magnification TEM image of an Fe_3O_4 nanotube, with the SEAD shown in the upper inset. (Lower inset) HRTEM images taken on the tube wall. (b) EDS spectra of solid (black curve) and hollow (red curve) part of a partial etched Fe_3O_4 nanotube (c).

resulted in Fe_3O_4 nanotubes with partially etched cores. The TEM image in Figure 3c clearly illustrates the details of such structures, where the hollow (upper) and solid (lower) regions are well-separated by a sharp domed-shape interface. This indicates that the action of capillary force plays a critical role during the etching process. Local EDS measurements performed at different sites along this half-etched structure has been demonstrated as the most direct way to inspect and verify the etching process. We demonstrated two EDS spectra in Figure 3b, which were taken in the upper and lower region of the nanowire in Figure 3c, respectively. It was found that the Mg signal from the hollow part (black curve) was significantly suppressed as compared with that from the solid region (red curve).

These free-standing Fe_3O_4 nanotubes have rendered a unique opportunity to investigate the electron transport through Fe_3O_4 in a quasi-one-dimensional form. In the last part of this report, we present electronic transport studies carried out with the Fe_3O_4 nanotubes. To set up a four-probe resistance measurement, e-beam lithography and evaporation were used to pattern and deposit four Ti/Au electrodes to contact individual nanotubes.⁷ I - V curves recorded at different temperatures (Figure 4a) exhibited rather linear feature, and the nanotube resistivity increased monotonically with the decreasing temperature. Room-temperature resistivity was deduced as $4 \times 10^{-2} \Omega \text{ cm}$ for the Fe_3O_4 nanotube, which is in good agreement with the value for epitaxial Fe_3O_4 thin films.⁸ The four-probe resistance (R) was also recorded as a function of temperature (T) (Figure 4a, inset). The rather linear relation in the Arrhenius plot ($\log R \approx 1/T$) suggested a thermally activated transport mechanism, with an activation energy derived to be ~ 0.1 eV. Due to spin-polarized transport across the structural domain

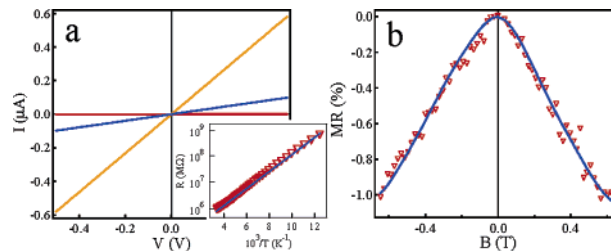


Figure 4. Electrical measurements of individual Fe_3O_4 nanotubes. (a) I - V curves taken at three different temperatures of 290 K (orange), 180 K (blue), and 77 K (red). (Inset) Arrhenius plot ($\log R \approx 1/T$) and its linear fitting (blue line). (b) MR measurement at 77 K. Data points are depicted as the red triangles with the blue curve as a guide for the eyes.

boundaries in Fe_3O_4 , magnetoresistance (MR) has also been observed in the Fe_3O_4 nanotubes (Figure 4b). MR of $\sim 1\%$ was observed at $T = 77$ K when a magnetic field of $B = 0.7$ T was applied parallel to the nanotube.

In summary, we report the first preparation of single-crystal Fe_3O_4 nanotubes using a wet-chemical etching method. Material characterization and fundamental transport studies have been presented. It is also worthwhile to emphasize that the dimension of these nanotubes, i.e., the length, inner diameter, and wall thickness, can be easily and independently controlled by tuning the length and diameter of the MgO cores and the deposition time/rate of the shell. More importantly, this method can be readily extended to a variety of materials that possess a close lattice match with MgO to produce intriguing nanostructures such as superconductive (e.g., YBCO) and piezoelectric (e.g., PZT) single-crystalline nanotubes.

Acknowledgment. We gratefully acknowledge support from a NSF CAREER Award, a NSF-CENS grant, and a SRC MARCO/DARPA grant. Z.L. thanks the University of Southern California for the “WISE” postdoctoral fellowship.

Supporting Information Available: Additional information on PLD and device fabrication processes. This material is available free of charge via the Internet at <http://pubs.acs.org>.

References

- (1) (a) Fan, R.; Wu, Y.; Li, D.; Yue, M.; Majumda, A.; Yang, P. *J. Am. Chem. Soc.* **2003**, *125*, 5254. (b) Daiguji, H.; Yang, P.; Majumdar, A. *Nano Lett.* **2004**, *4*, 137. (c) Sui, Y. C.; Skomski, R.; Sorge, K. D.; Sellmyer D. J. *J. Appl. Phys.* **2004**, *95*, 7151. (d) Li, D.; Xia, Y. *Nano Lett.* **2004**, *4*, 933. (e) Hueso, L.; Mathur, N. *Nature* **2004**, *427*, 301. (f) Ding, Y.; Kong, X. Y.; Wang, Z. L. *J. Appl. Phys.* **2004**, *95*, 306. (g) Goldberger, J.; He, R.; Zhang, Y.; Lee, S.; Yan, H.; Chio, H.; Yang, P. *Nature* **2003**, *422*, 599.
- (2) Levy, P.; Leyva, A. G.; Troiani, H. E.; Sanchez, R. D. *Appl. Phys. Lett.* **2003**, *83*, 5247.
- (3) Skomski, R. *J. Phys.: Condens. Matter* **2003**, *15*, R841.
- (4) Rao, C. N. R.; Nath, M. *Dalton Trans.* **2003**, 1.
- (5) Aharoni, A. *Introduction to the Theory of Ferromagnetism*; Oxford University Press: New York, 1996.
- (6) (a) Han, S.; Li, C.; Liu, Z.; Lei, B.; Zhang, D.; Jin, W.; Liu, X.; Tang, T. *Nano Lett.* **2004**, *4*, 1241. (b) Zhang, D.; Liu, Z.; Han, S.; Li, C.; Lei, B.; Stewart M. P.; Tour, J. M.; Zhou, C. *Nano Lett.* **2004**, *4*, 2151.
- (7) See Supporting Information.
- (8) (a) Eerenstein, W.; Palstra, T. T. M.; Hibma, T.; Celitto, S. *Phys. Rev. B* **2002**, *66*, 221101. (b) Sena, S. P.; Lindley, R. A.; Blythe, H. J.; Sauer, Ch.; Al-Kafarji, M.; Gehring, G. A. *J. Magn. Mater.* **1997**, *176*, 111. (c) Kim, W.; Kawaguchi, K.; Koshizaki, N.; Sohma, M.; Mastsumoto, T. *J. Appl. Phys.* **2003**, *93*, 8032.

JA0445239